HOKKAIDO UNIVERSITY

Title	Genome-wide DNA methylation profile in feline haematological tumours: A preliminary study
Author(s)	Yamazaki, Jumpei; Jelinek, Jaroslav; Yokoyama, Shoko et al.
Citation	Research in veterinary science, 140, 221-228 https://doi.org/10.1016/j.rvsc.2021.09.002
Issue Date	2021-11
Doc URL	https://hdl.handle.net/2115/87058
Rights	© 2021. This manuscript version is made available under the CC-BY-NC-ND 4.0 license https://creativecommons.org/licenses/by-nc-nd/4.0/
Type	journal article
File Information	Research in veterinary science140_221-228.pdf

Hokkaido University Collection of Scholarly and Academic Papers : HUSCAP

REVISED Manuscript (text UNmarked) Click here to view linked References

Original Article

Genome-wide DNA methylation profile in feline haematological tumours: a preliminary study

Jumpei Yamazaki [a,b*], Jaroslav Jelinek [c], Shoko Yokoyama [a], Mitsuyoshi Takiguchi [a]

[a] *Veterinary Teaching Hospital, Graduate School of Veterinary Medicine, Hokkaido University, Japan*

[b] *One Health Research Center, Hokkaido University, Japan.*

[c] *Coriell Institute for Medical Research, Camden, NJ, USA.*

Keywords: DNA methylation, Epigenetics, Cat, Next generation sequencing

Abbreviations

CGI

CpG islands

DREAM

Digital Restriction Enzyme of DNA Methylation Analysis

* Corresponding author. Tel.: +81 11 706 5319
E-mail address: j.yamazaki@vetmed.hokudai.ac.jp (J. Yamazaki).

Abstract

Although DNA methylation has been analysed in few studies for a limited number of loci in cats with diseases, genome-wide profile of DNA methylation has never been addressed. The hypothesis for this study is that next-generation sequencing with sequential digestion of genomic DNA with *Sma*I and *Xma*I enzymes could provide highly quantitative information on methylation levels in cats.

Using blood from four healthy control cats and two disease cats as well as three feline lymphoma/leukemia cell lines, approximately 74-94 thousand CpG sites across the cat genome could be analysed. CpG sites in CpG island (CGI) CGI broadly were either methylated or unmethylated in normal blood, while CpG sites in non-CpG islands (NCGI) are largely methylated. Lymphoma cell lines showed thousands of CpG sites with gain of methylation at normally unmethylated CGI sites and loss of methylation at normally methylated NCGI sites. Hypermethylated CpG sites located at promoter regions included genes annotated with 'developmental process' and 'anatomical structure morphogenesis' such as *HOXD10*. This highly quantitative method would be suitable for studies of DNA methylation changes not only in cancer but also in other common diseases in cats.

Introduction

DNA methylation is a covalent modification involving the addition of methyl groups at cytosine–guanine (CpG) dinucleotides, which converts cytosine to 5-methylcytosine (5mC). CpGs are rare and scattered throughout the genome (Klose and Bird, 2006), and also exist as CpG-rich regions (CpG islands; CGIs) (Illingworth and Bird, 2009). CGIs are one of the most important methylation features of the genome and are methylated differently from non-CpG islands (NCGIs) in mammals (Bird, 2002). Indeed, most CpGs in non-CpG islands (NCGI) are fully methylated while CpG dinucleotides in CGIs are typically unmethylated. Furthermore, CGI methylation is associated with silencing of the associated promoter, as seen in imprinting and the inactive X chromosome in women (Ferguson-Smith, 2011; Heard et al., 1997).

DNA methylation plays a key role in disease mechanisms such as tumourigenesis, where the *de novo* hypermethylation of tumour suppresser genes has been identified in neoplastic tissues (Herman et al., 1994; Merlo et al., 1995). Global hypomethylation also occurs frequently in tumours and may facilitate chromosome instability, leading to the formation of abnormal chromosomal structures (Eden et al., 2003). Recent advances in genome-wide analysis of DNA methylation have revealed the occurrence of aberrant methylation in a variety of human diseases (Figueroa et al., 2009; Noushmehr et al., 2010). Moreover, hypermethylated sites have been identified at promoter regions in feline lymphoma and squamous cell carcinoma (Fujita and Kaneda, 2017; Morandi et al., 2020; Renzi et al., 2020). However, these studies focused on target genes or regions of DNA methylation extrapolated from human work, indicating the reduced capability of screening affected genes or regions in cats. The genome-wide screening of regions with DNA methylation changes in feline diseases is required to clarify disease mechanisms and to establish a novel marker for diagnosis and prognosis in clinical settings.

We hypothesised that genome-wide DNA methylation analysis can provide a highly quantitative assessment of DNA methylation levels in cats. To investigate this, we used next-generation sequencing with sequential *Sma* I and *Xma* I digestion of genomic DNA to analyse methylation levels in blood from healthy control and diseased cats as well as in feline lymphoma cell lines.

Materials and methods

Cell lines and normal blood

We analysed three lymphoma cell lines (T-cell type, FT1, KO1; B-cell type, MS4) (Fujino et al., 2004; Miura et al., 1987; Mochizuki et al., 2011b). Peripheral blood samples were obtained from four healthy volunteer cats (NM1, 4-year-old female American short hair; NM2, 5-year-old male mixed; NM3 and NM4, 8-month-old male mixed). All these cats were considered healthy on the basis of results of a baseline physical examination and CBC. We also used peripheral blood samples from two disease cats diagnosed as having lymphoma (SHT, cell lineage not determined by PCR for antigen receptor gene rearrangement (Mochizuki et al., 2011a; Mochizuki et al., 2012)) and acute myelogenous leukemia (KYK), respectively.

Digital restriction enzyme analysis of methylation (DREAM)

Genome-wide DNA methylation analysis using next-generation sequencing was performed according to the corresponding studies in human (Jelinek et al., 2012) as well as in dog (Yamazaki et al., 2018) (Fig. 1). Briefly, genomic DNA extracted from the samples was mixed with a set of artificial methylation standards for calibrators (methylation levels of 0%, 25%, 50%, 75% and 100%). These mixes were digested with 100 U of *Sma*I endonuclease (New England Biolabs) for 8 h at 25 °C. Subsequently, 50 U of *Xma*I endonuclease (New England Biolabs) were added, and the digestion continued for an additional 16 h at 37 °C. The 3′ recessed

ends of the DNA created by XmaI digestion were filled in a dCTP, dGTP, and dATP mix (0.4 mM of each) and 3′-dA tails were added to all restriction fragments by Klenow DNA polymerase lacking 3′-to-5′ exonuclease activity (New England Biolabs). Then, Illumina paired-end sequencing adaptors were ligated using T4 DNA ligase (New England Biolabs) followed by size-selection with Agencourt AMPure XP magnetic beads for DNA fragments ranging from 250 bp to 450 bp in size. Size-selected DNA was amplified with paired-end PCR primers (Illumina) using KAPA Hifi HotStart ReadyMix (Kapa Biosystems) and 11 cycles of amplification followed by sequencing on NovaSeq (Illumina). Sequencing reads were mapped to *Sma*I/*Xma*I sites in the cat genome (felCat9), and signatures corresponding to methylated and unmethylated CpGs were enumerated to calculate methylation frequencies for individual *Sma*I/*Xma*I site. The methylation ratio is the ratio of the number of tags starting with CCGGG divided by the total number of tags mapped to a given *Sma*I/*Xma*I site. Finally, we corrected methylation levels measured by DREAM based on the values obtained from the spikes in standards. First, we calculated log ratios ln (m/u) and ln (sm/u) for each standard, where m/u is the expected ratio of methylated and unmethylated reads, while sm and u, respectively, are observed numbers of methylated and unmethylated reads. Differences in the 'expected' minus 'observed' log ratios were calculated for each standard. Correction factor c was calculated as an antilog of the average log difference (expected – observed). Corrected methylation values were then computed as $100\% \times [c \times sm/(c \times sm+u)]$ for each CpG site.

We used the University of California, Santa Cruze (UCSC) definition of CpG islands (Gardiner-Garden and Frommer, 1987). Promoter regions are defined as being located within 1 kb from transcription start sites (TSS) of given genes annotated by Ensembl Gene Predictions – version 101 (Liu et al., 2018; Noguchi et al., 2020). Only autosomal CpG sites were analysed.

Gene ontology analysis

Gene ontology (GO) analysis of differentially methylated genes was done using the PANTHER (Mi et al., 2021) and analyses were performed online using parameters of false discovery rate of $<5 \times 10^{-2}$.

Results

CpG site analysis

From all nine samples used for DREAM, 5.2–12.8 million unique, usable sequencing reads were successfully generated after conservative filtering for DNA methylation analyses (Table 1). CpG sites with more than 20 reads (74,000–94,000 CpG sites per sample) were utilised to assure quantitative ability and intersample comparisons.

We obtained DNA methylation levels for two CpG sites at the *SOX11* promoter region of 98.3% and 99.1% in the FT-1 cell line, and 0.0% and 0.0% in the MS4 cell line. This compares with DNA methylation levels of the *SOX11* promoter region achieved by bisulfite sequencing of 92.2% and 11.7% in FT-1 and MS4 cell lines, respectively (Fujita and Kaneda, 2017).

Next, we analysed 38,930 CpG sites with more than 20 reads in all nine samples to compare DNA methylation differences. Of the 38,930 CpG sites, 2843 (7.3%) were located close to promoter regions, 4537 (11.7%) were within exons, and 16,811 (43.2%) were within introns. The remaining 14,739 CpG sites were distant from any genes except for 730 sites located within non-coding RNAs such as long non-coding RNAs (Fig. 2). A total of 20,242 CpG sites were in CGIs and 18,688 in NCGIs.

DNA methylation patterns

Next, we addressed overall DNA methylation levels. Average DNA methylation levels ranged from 33.1%–67.2% (Table 1). Fig. 3 shows DNA methylation fractions and the overall distribution of DNA methylation levels. Most CpG sites were either highly methylated (>80%) or unmethylated (<20%) in all samples. Interestingly, we detected a high degree of hypomethylation in MS4 cells compared with other cells, and moderate hypomethylation in one diseased cat compared with other cats.

To address if genome-wide DNA methylation analysis could differentiate the methylation status of all samples, we calculated the correlation coefficient for all pairs (n=36) of samples analysed. As expected, high correlations (R = 0.987–0.991) were observed in all pairs of healthy control cats and to a lesser extent in the pairs of controls with diseased cats (R = 0.927–0.977) (Fig. 4A). However, lower correlations were observed for the three cell lines (R = 0.437–0.695). MS4 cells typically showed lower correlations with other samples whereas the other two cell lines showed higher correlations (R = 0.784).

Genome-wide DNA methylation patterns in the present study were sufficiently variable to identify sample differences, indicating that methylation levels for CpG sites varied among samples. Fig. 5 shows representative scatter plots for CpG sites in CGIs and NCGIs for one healthy control cat, one diseased cat, and two cell lines compared with another healthy control cat. In support of earlier findings, DNA methylation levels in the blood of two healthy control cats were highly consistent both for CGIs and NCGIs. However, major differences were detected between CGI and NCGI CpG sites. More CGI CpG sites were unmethylated (DNA methylation levels, <20%) than methylated (DNA methylation levels, >80%). In contrast, methylated CpG sites were dominant in NCGIs. One diseased cat showed hypermethylated CpG sites in tumour samples that were unmethylated in whole blood as well as hypomethylated CGI and NCGI CpG sites in tumour samples that were methylated in whole blood (Fig. 5).

Additionally, two lymphoma cell lines showed higher degrees of hypermethylation (more apparent in KO1) and hypomethylation (more apparent in MS4).

Differentially methylated CpG sites

To gain insights into the DNA methylation of CpG sites that showed variation between tumour samples and healthy controls, we calculated the number of CpG sites that either gained methylation (higher than the average + 2 standard deviation [SD] of DNA methylation levels in four control cats) or lost methylation (lower than the average – 2SD of DNA methylation levels in four control cats) in diseased cats and lymphoma cell lines. We found that 1323–7852 CpG sites (6.5%–38.8%) of those CGI CpG sites analysed increased methylation in different cell lines (Table 2). Interestingly, KO1 and FT1 cell lines had more hypermethylated CpG sites than other cell lines. We also found that 2728–13,876 CpG sites (14.6%–74.3%) of the NCGI CpG sites analysed were hypomethylated (Table 2). MS4 cells had many more hypomethylated CpG sites than other cell lines.

Hypermethylation in promoter regions is a well-known phenomenon that correlates with gene silencing (Jones and Baylin, 2007). We used the criterion of defining differential hypermethylation as more than a 20% difference in DNA methylation level for given CpG sites (Guo et al., 2014; Vorjohann et al., 2013) in tumour samples compared with healthy controls to identify 7223, 2906, and 7725 CpG sites as being differentially hypermethylated in KO1, MS4, and FT1 cell lines, respectively; two diseased cats showed smaller numbers of differential hypermethylation (1695 and 84 CpG sites). We then confirmed their genomic coordinates to determine the biological relevance of DNA methylation changes in lymphoma cell lines. Fig. 6A shows that the two CpGs that could be analysed in this study set (chrC1: 166,885,535 and 166,885,769) are close to each other and showed similar trends of DNA methylation. Both CpG sites were hypermethylated (56%–100%) in the cell lines but unmethylated (0%–11%) in

diseased and healthy control cats. Interestingly, both sites are located at the promoter region of the cat *HOXD10* gene. Finally, we found that three cell lines had 2121 commonly differentially hypermethylated CpG sites (Fig. 6B), including within 185 genes with differential promoter hypermethylation. GO analysis of these 185 genes showed that the majority were associated with the GO biological process of 'developmental process' and 'anatomical structure morphogenesis' (Supplementary Table 1).

Discussion

Genome-wide DNA methylation analysis by next-generation sequencing has both advantages and disadvantages (Barros-Silva et al., 2018). Antibodies against 5-mC or methyl-binding proteins can be combined with sequencing, but this does not permit the methylation status of individual CpG sites to be ascertained. Moreover, high sequencing costs associated with the shotgun sequencing approach of bisulfite-converted whole genomes hampers research applications and progress. Therefore, obtaining a DNA methylome with a single-base resolution or wide coverage is impractical, especially in the field of companion animals where DNA methylation studies are still in their infancy. Given this, we established a novel method of measuring DNA methylation in the cat genome based on methylation-specific signatures using methylation sensitive/insensitive restriction enzymes combined with next-generation sequencing. This approach has already been applied to humans as DREAM (Jelinek et al., 2012) as well as dogs as canine DREAM (Yamazaki et al., 2018), and successfully identified aberrant DNA methylation in tumours in each species (Ishizaki et al., 2020; Ohta et al., 2020; Yamazaki et al., 2015). We used it here to quantitatively determine the DNA methylation status of 38,930 CpG sites in nine samples, including 2843 (7.3%) CpG sites located close to the promoter regions of predicted cat genes.

We validated our DNA methylation statuses by comparing them with bisulfite sequencing findings from a previous study (Fujita and Kaneda, 2017), and demonstrated a high correlation for the *SOX11* promoter region between the two analyses. This was despite the fact that the CpG sites analysed in the two studies differed, being 3.6 kb upstream from the transcription start site in the bisulfite sequencing study and 86 bp and 253 bp upstream from the transcription start site in our study. A further advantage of our method over conventional bisulfite sequencing is shown by the number of sequencing reads achieved. We used CpG sites with at least 20 reads, and obtained approximately 100 reads for the *SOX11* promoter compared with the bisulfite sequencing of only 12 clones, suggesting a higher quantitative capacity and accuracy of our method.

The overall DNA methylation status in our study indicated that most CpG sites were either highly methylated (>80%) or unmethylated (<20%) in all samples. Approximately 50% of CpG sites were methylated regardless of the cell type analysed, whereas 30% of CpG sites were unmethylated (Fig. 3). Interestingly, we also found that MS4 and KYK cell lines were hypomethylation-prone compared with other cell lines and the four healthy control cats, which is consistent with the finding in canine lymphoma cell lines where two out of five samples showed a strong hypomethylation phenotype (Yamazaki et al., 2018). Furthermore, we found strikingly different characteristics at CGI and NCGI CpG sites. Most CGI CpG sites were unmethylated (DNA methylation levels, <20%) or methylated (DNA methylation levels, >80%), while methylated NCGI CpG sites dominated. These findings are also consistent with previous studies in humans (Jelinek et al., 2012) and dogs (Yamazaki et al., 2018).

Although the distribution of DNA methylation levels appeared similar in all samples, we found that genome-wide DNA methylation patterns differed (Fig. 4). This indicated that methylation levels at each CpG site varied sufficiently to show identifying characteristics. To confirm this, we studied differentially methylated CpG sites between healthy and diseased

samples, and detected methylation gains at normally unmethylated CGI sites and methylation losses at normally methylated NCGI sites, similar to findings in human tumours (Taby and Issa, 2010) and dog tumours (Ishizaki et al., 2020). Furthermore, DNA methylation patterns varied among diseased samples. For example, KO1 and FT1 cell lines showed a higher number of hypermethylated CGI CpG sites compared with other samples, while MS4 cells had the highest number of hypomethylated NCGI CpG sites followed by KYK cells. This implies that differentially methylated CpG sites are affected by individual tumour characteristics.

There are several lines of possibilities to explain this finding. First, we used a variety of sample phenotypes including T-cells (KO1 and FT1), B-cells (MS4), myeloid cells, and undetermined lineages. In human lymphoma, differential methylation has been reported between B-cells and T-cells, depending on the lymphoma subtype, as well as even among the same immunological phenotypes (Bergmann et al., 2019; Nakamura et al., 2017; Shaknovich et al., 2010). However, methylation patterns of blood samples from several healthy control cats were nearly identical in our study, suggesting a conserved methylation status despite the presence of different cell types. Alternatively, DNA methylation levels could be affected by the tumour cell purity in a population context-manner. While cell lines are comprised of tumour cells only, blood samples from clinical cases contain different numbers of normal blood cells depending on the patients' condition. Therefore, sample DNA methylation levels might be less representative than those of tumour cells alone. To overcome this problem, future studies would ideally conduct a cell sorting strategy to isolate only tumour cells if appropriate markers and antibodies are available for feline tumours.

A variety of aberrant DNA methylation types has been reported in human patients with the same subtype of certain tumours. For example, the CpG island methylator phenotype (CIMP) was found in most human tumours where a subset of CpG sites was unequivocally and uniformly hypermethylated (Noushmehr et al., 2010; Toyota et al., 1999), and patients with

CIMP share the same clinicopathological features of these tumours (Enjuanes et al., 2011). Interestingly, we found remarkable overlaps of hypermethylated sites even among cell lines in our study. However, this is a preliminary report with a limited number of samples. Further investigation with more clinical cases is required to elucidate the association between differential methylation and prognosis or the cell phenotype of feline tumours.

We detected promoter hypermethylation in 185 genes common to all three cell lines, for which annotations of the terms 'developmental process' and 'anatomical structure morphogenesis' including *HOXD10* were enriched. This indicated a possible common mechanism for gene silencing by aberrant hypermethylation, although long-term cultured normal cells have been reported to show changes in the DNA methylation of homeobox genes (Bork et al., 2010). To further address this question, it will be necessary to test the functional relevance of these methylated CpG sites by examining gene expression levels.

Conclusion

In conclusion, we established a genome-wide analysis of DNA methylation based on next-generation sequencing in cats which allowed us to identify thousands of aberrant DNA methylation in blood from haematological tumours. The highly quantitative method would be suitable for studies of DNA methylation changes not only in cancer but also in other common diseases in cats.

Conflicts of Interest statement

None of the authors has any financial or personal relationships that could inappropriately influence or bias the content of the paper.

Acknowledgements

The authors would like to thank Dr. Yuko Goto-Koshino (The University of Tokyo, Japan) for generously providing the KO1, MS4, and FT1 cell lines. The authors would also like to thank the owners of healthy control cats for generously providing normal peripheral blood of those cats. This work was supported by JSPS KAKENHI Grant Number 18K05964 and 21H02351. This work was also supported by the World-leading Innovative and Smart Education (WISE) Program (1801) from the Ministry of Education, Culture, Sports, Science, and Technology, Japan.

Reference

Barros-Silva, D., Marques, C.J., Henrique, R., Jeronimo, C., 2018. Profiling DNA Methylation Based on Next-Generation Sequencing Approaches: New Insights and Clinical Applications. Genes (Basel) 9.

Bergmann, A.K., Fataccioli, V., Castellano, G., Martin-Garcia, N., Pelletier, L., Ammerpohl, O., Bergmann, J., Bhat, J., Pau, E.C.S., Martin-Subero, J.I., Moffitt, A.B., Valencia, A., Oberg, H.H., Wesch, D., Jayne, S., Dyer, M.J.S., Kabelitz, D., Gaulard, P., Siebert, R., 2019. DNA methylation profiling of hepatosplenic T-cell lymphoma. Haematologica 104, e104-e107.

Bird, A., 2002. DNA methylation patterns and epigenetic memory. Genes and Development 16, 6-21.

Bork, S., Pfister, S., Witt, H., Horn, P., Korn, B., Ho, A.D., Wagner, W., 2010. DNA methylation pattern changes upon long-term culture and aging of human mesenchymal stromal cells. Aging Cell 9, 54-63.

Eden, A., Gaudet, F., Waghmare, A., Jaenisch, R., 2003. Chromosomal instability and tumors promoted by DNA hypomethylation. Science 300, 455.

Enjuanes, A., Fernandez, V., Hernandez, L., Navarro, A., Bea, S., Pinyol, M., Lopez-Guillermo, A., Rosenwald, A., Ott, G., Campo, E., Jares, P., 2011. Identification of methylated genes associated with aggressive clinicopathological features in mantle cell lymphoma. PloS One 6, e19736.

Ferguson-Smith, A.C., 2011. Genomic imprinting: the emergence of an epigenetic paradigm. Nat Rev Genet 12, 565-575.

Figueroa, M.E., Skrabanek, L., Li, Y., Jiemjit, A., Fandy, T.E., Paietta, E., Fernandez, H., Tallman, M.S., Greally, J.M., Carraway, H., Licht, J.D., Gore, S.D., Melnick, A., 2009. MDS and secondary AML display unique patterns and abundance of aberrant DNA methylation. Blood 114, 3448-3458.

Fujino, Y., Ma, Z., Satoh, H., Mizuno, T., Hisasue, M., Baba, K., Masuda, K., Ohno, K., Onishi, T., Tsujimoto, H., 2004. Characterization of a newly established nonproducer lymphoma cell line for feline leukemia virus. Veterinary Immunology and Immunopathology 102, 429-439.

Fujita, M., Kaneda, M., 2017. DNA methylation inhibitor causes cell growth retardation and gene expression changes in feline lymphoma cells. Journal of Veterinary Medical Science 79, 1352-1358.

Gardiner-Garden, M., Frommer, M., 1987. CpG islands in vertebrate genomes. Journal of Molecular Biology 196, 261-282.

Guo, H., Zhu, P., Yan, L., Li, R., Hu, B., Lian, Y., Yan, J., Ren, X., Lin, S., Li, J., Jin, X., Shi, X., Liu, P., Wang, X., Wang, W., Wei, Y., Li, X., Guo, F., Wu, X., Fan, X., Yong, J., Wen, L., Xie, S.X., Tang, F., Qiao, J., 2014. The DNA methylation landscape of human early embryos. Nature 511, 606-610.

Heard, E., Clerc, P., Avner, P., 1997. X-chromosome inactivation in mammals. Annual Review of Genetics 31, 571-610.

Herman, J.G., Latif, F., Weng, Y., Lerman, M.I., Zbar, B., Liu, S., Samid, D., Duan, D.S., Gnarra, J.R., Linehan, W.M., et al., 1994. Silencing of the VHL tumor-suppressor gene by DNA methylation in renal carcinoma. Proceedings of the National Academy of Sciences of the United States of America 91, 9700-9704.

Illingworth, R.S., Bird, A.P., 2009. CpG islands--'a rough guide'. FEBS Letters 583, 1713-1720.

Ishizaki, T., Yamazaki, J., Jelinek, J., Aoshima, K., Kimura, T., 2020. Genome-wide DNA methylation analysis identifies promoter hypermethylation in canine malignant melanoma. Research in Veterinary Science 132, 521-526.

Jelinek, J., Liang, S., Lu, Y., He, R., Ramagli, L.S., Shpall, E.J., Estecio, M.R., Issa, J.P., 2012. Conserved DNA methylation patterns in healthy blood cells and extensive changes in leukemia measured by a new quantitative technique. Epigenetics 7, 1368–1378.

Jones, P.A., Baylin, S.B., 2007. The epigenomics of cancer. Cell 128, 683-692.

Klose, R.J., Bird, A.P., 2006. Genomic DNA methylation: the mark and its mediators. Trends in Biochemical Sciences 31, 89-97.

Liu, J., Arabaciyan, S., Francois, J.M., Capp, J.P., 2018. Bimodality of gene expression from yeast promoter can be instigated by DNA context, inducing conditions and strain background. FEMS Yeast Res 18.

Merlo, A., Herman, J.G., Mao, L., Lee, D.J., Gabrielson, E., Burger, P.C., Baylin, S.B., Sidransky, D., 1995. 5' CpG island methylation is associated with transcriptional silencing of the tumour suppressor p16/CDKN2/MTS1 in human cancers. Nature Medicine 1, 686-692.

Mi, H., Ebert, D., Muruganujan, A., Mills, C., Albou, L.P., Mushayamaha, T., Thomas, P.D., 2021. PANTHER version 16: a revised family classification, tree-based classification tool, enhancer regions and extensive API. Nucleic Acids Research 49, D394-D403.

Miura, T., Tsujimoto, H., Fukasawa, M., Kodama, T., Shibuya, M., Hasegawa, A., Hayami, M., 1987. Structural abnormality and over-expression of the myc gene in feline leukemias. International Journal of Cancer 40, 564-569.

Mochizuki, H., Nakamura, K., Sato, H., Goto-Koshino, Y., Sato, M., Takahashi, M., Fujino, Y., Ohno, K., Uchida, K., Nakayama, H., Tsujimoto, H., 2011a. Multiplex PCR and Genescan analysis to detect immunoglobulin heavy chain gene rearrangement in feline B-cell neoplasms. Veterinary Immunology and Immunopathology 143, 38-45.

Mochizuki, H., Nakamura, K., Sato, H., Goto-Koshino, Y., Sato, M., Takahashi, M., Fukushima, K., Nakashima, K., Fujino, Y., Ohno, K., Uchida, K., Nakayama, H., Tsujimoto, H., 2012. GeneScan analysis to detect clonality of T-cell receptor gamma gene rearrangement in feline lymphoid neoplasms. Veterinary Immunology and Immunopathology 145, 402-409.

Mochizuki, H., Takahashi, M., Nishigaki, K., Ide, T., Goto-Koshino, Y., Watanabe, S., Sato, H., Sato, M., Kotera, Y., Fujino, Y., Ohno, K., Uchida, K., Tsujimoto, H., 2011b. Establishment of a novel feline leukemia virus (FeLV)-negative B-cell cell line from a cat with B-cell lymphoma. Veterinary Immunology and Immunopathology 140, 307-311.

Morandi, L., Sabattini, S., Renzi, A., Rigillo, A., Bettini, G., Dervas, E., Schauer, A., Morandi, M., Gissi, D.B., Tarsitano, A., Evangelisti, S., Tonon, C., 2020. An Evolutionary Cancer Epigenetic Approach Revealed DNA Hypermethylation of Ultra-Conserved Non-Coding Elements in Squamous Cell Carcinoma of Different Mammalian Species. Cells 9.

Nakamura, T., Yamashita, S., Fukumura, K., Nakabayashi, J., Tanaka, K., Tamura, K., Tateishi, K., Kinoshita, M., Fukushima, S., Takami, H., Fukuoka, K., Yamazaki, K., Matsushita, Y., Ohno, M., Miyakita, Y., Shibui, S., Kubo, A., Shuto, T., Kocialkowski, S., Yamanaka, S., Mukasa, A., Sasayama, T., Mishima, K., Maehara, T., Kawahara, N., Nagane, M., Narita, Y., Mano, H., Ushijima, T., Ichimura, K., 2017. Genome-wide DNA methylation profiling identifies primary central nervous system lymphoma as a distinct entity different from systemic diffuse large B-cell lymphoma. Acta Neuropathologica 133, 321-324.

Noguchi, H., Miyagi-Shiohira, C., Nakashima, Y., Kinjo, T., Saitoh, I., Watanabe, M., 2020. Mutations in the C1 element of the insulin promoter lead to diabetic phenotypes in homozygous mice. Commun Biol 3, 309.

Noushmehr, H., Weisenberger, D.J., Diefes, K., Phillips, H.S., Pujara, K., Berman, B.P., Pan, F., Pelloski, C.E., Sulman, E.P., Bhat, K.P., Verhaak, R.G., Hoadley, K.A., Hayes, D.N., Perou, C.M., Schmidt, H.K., Ding, L., Wilson, R.K., Van Den Berg, D., Shen, H., Bengtsson, H., Neuvial, P., Cope, L.M., Buckley, J., Herman, J.G., Baylin, S.B., Laird, P.W., Aldape, K., Cancer Genome Atlas Research, N., 2010. Identification of a CpG island methylator phenotype that defines a distinct subgroup of glioma. Cancer Cell 17, 510-522.

Ohta, H., Yamazaki, J., Jelinek, J., Ishizaki, T., Kagawa, Y., Yokoyama, N., Nagata, N., Sasaki, N., Takiguchi, M., 2020. Genome-wide DNA methylation analysis in canine gastrointestinal lymphoma. Journal of Veterinary Medical Science 82, 632-638.

Renzi, A., Morandi, L., Lenzi, J., Rigillo, A., Bettini, G., Bellei, E., Giacomini, A., Tinto, D., Sabattini, S., 2020. Analysis of DNA methylation and TP53 mutational status for differentiating feline oral squamous cell carcinoma from non-neoplastic mucosa: A preliminary study. Veterinary and Comparative Oncology 18, 825-837.

Shaknovich, R., Geng, H., Johnson, N.A., Tsikitas, L., Cerchietti, L., Greally, J.M., Gascoyne, R.D., Elemento, O., Melnick, A., 2010. DNA methylation signatures define molecular subtypes of diffuse large B-cell lymphoma. Blood 116, e81-89.

Taby, R., Issa, J.P., 2010. Cancer epigenetics. CA: A Cancer Journal for Clinicians 60, 376-392.

Toyota, M., Ahuja, N., Ohe-Toyota, M., Herman, J.G., Baylin, S.B., Issa, J.P., 1999. CpG island methylator phenotype in colorectal cancer. Proceedings of the National Academy of Sciences of the United States of America 96, 8681-8686.

Vorjohann, S., Pitetti, J.L., Nef, S., Gonelle-Gispert, C., Buhler, L., Fish, R.J., Neerman-Arbez, M., 2013. DNA methylation profiling of the fibrinogen gene landscape in human cells and during mouse and zebrafish development. PloS One 8, e73089.

Yamazaki, J., Jelinek, J., Hisamoto, S., Tsukamoto, A., Inaba, M., 2018. Dynamic changes in DNA methylation patterns in canine lymphoma cell lines demonstrated by genome-wide quantitative DNA methylation analysis. Veterinary Journal 231, 48-54.

Yamazaki, J., Jelinek, J., Lu, Y., Cesaroni, M., Madzo, J., Neumann, F., He, R., Taby, R., Vasanthakumar, A., Macrae, T., Ostler, K.R., Kantarjian, H.M., Liang, S., Estecio, M.R., Godley, L.A., Issa, J.P., 2015. TET2 mutations affect non-CpG island DNA methylation at enhancers and transcription factor binding sites in chronic myelomonocytic leukemia. Cancer Research.

Table 1

The numbers of unique usable reads for each sample (n = 9) following DREAM (digital restriction enzyme analysis of methylation) and CpG sites covered by more than 20 reads which were suitable for DNA methylation analysis. Peripheral blood samples were obtained from four healthy volunteer cats and two disease cats.

Samples	***Number of reads***	***Number of CpG Sites covered***	***Average CpG methylation***
KO1	10,764,905	74,135	67.2
MS4	11,644,221	94,168	33.1
FT1	12,841,323	92,971	67.1
SHT	9,530,327	84,941	59.0
KYK	6,850,336	89,229	53.2
NM1	9,912,124	93,645	59.4
NM2	11,812,510	84,157	59.0
NM3	6,303,747	81,425	58.2
NM4	5,274,508	75,079	58.2

Table 2

The numbers of hypermethylated sites in CpG islands (CGIs) and hypomethylated CpG sites in not in CGIs (NCGIs) in three different lymphoma cell lines and two disease cats compared to healthy control cats.

		KO1	MS4	FT1	SHT	KYK
CGI	Hypermethylated	7852	3411	7419	3066	1323
	Hypomethylated	1579	7294	2511	1608	5117
NCGI	Hypermethylated	5319	1461	3915	3119	603
	Hypomethylated	4057	13876	6087	2728	9408

448 **Figure Legends**

449

450 Fig. 1

451 Schematic outline of the DREAM principle. SmaI restriction endonuclease can cut only
452 unmethylated CCCGGG sites creating 5′ -GGG signatures. Remaining methylated
453 CCmeCGGG sites are then cut by XmaI restriction endonuclease creating 5′ -CCGGG
454 signatures. Sequencing adapters are ligated to SmaI/XmaI fragments and the libraries are
455 subjected to next generation sequencing. Methylation levels at unique SmaI/XmaI sites are
456 calculated based on the numbers of methylated and total signatures.

457

458 Fig. 2

459 Numbers of CpG sites analyzed in this study in each category of genomic features. C, CpG
460 island, N, Non-CpG island

461

462 Fig.3

463 Characterization of DNA methylation patterns across cell types

464 Violin plots of genome-wide DNA methylation levels of all CpG sites (a), sites in CpG islands
465 (c), and sites in non-CpG islands (e) for each sample.

466 Density plots of genome-wide DNA methylation levels of all CpG sites (b), sites in CpG islands
467 (d), and sites in non-CpG islands (f) for each sample.

468

469 Fig.4

470 Pairplot for Pearson's correlation scores of DNA methylation levels with all CpG sites
471 analyzed. Samples include blood from healthy control cats (green), disease cats (blue), and cell
472 lines (sky blue). Coloring indicates low correlation (blue) to high (red).

Fig. 5

Representative smoothscatter plots for DNA methylation levels. 20,242 CpG sites in CpG island (left) and 18,688 non-CpG island (right) are plotted separately. DNA methylation of blood from a healthy control cat (NM1) is plotted on the x-axis, DNA methylation levels of blood from a disease cat (SHT) or cell lines (KO1 and MS4) are plotted on the y-axis. The density in number of CpG sites increases from white to green to blue.

Fig. 6

Schematic representation of a representative genomic landscape or hypermethylated CpG sites in the cell lines. Original pictures were taken from the University of California, Santa Cruze (UCSC) browser[1]. Promoter regions of cat *HOXD10* are shown with DNA methylation levels for two CpG sites in each sample along with locations of CpG islands and the homologous genes of mouse and human. Note that these sites are on CGIs and are hypermethylated only in the cell lines but not in blood from healthy control cats. (b) Venn diagram showing the overlap of hypermethylated CpG sites among (a) KO1, MS4, and FT1.

[1] See: http://genome.ucsc.edu/cgi-bin/hgGateway

Click here to access/download;Figure;Figure.pdf

Fig. 1

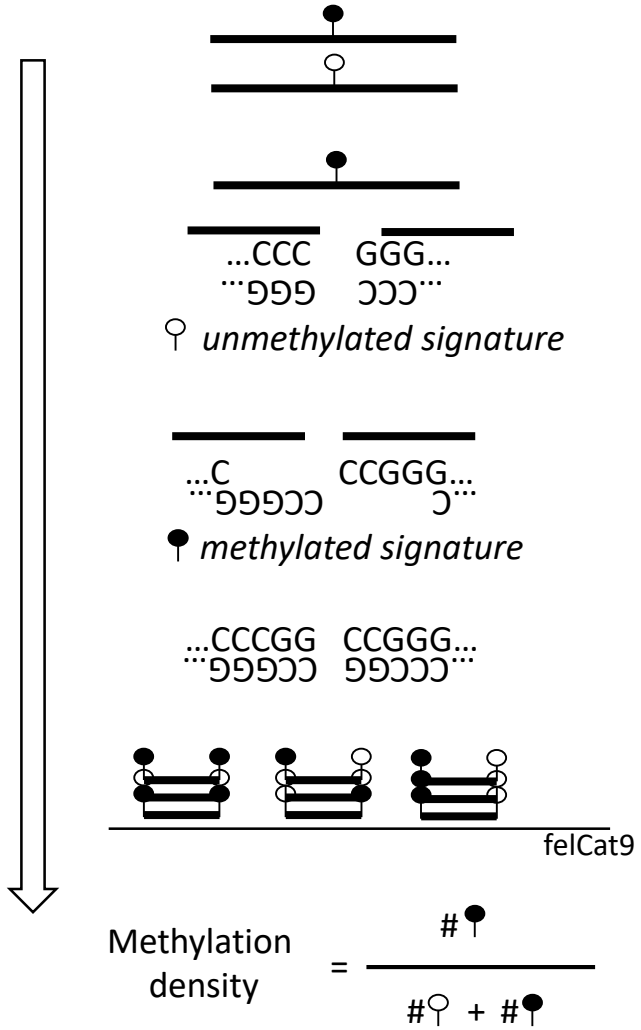

Mixture of DNA and artificial methylation standards with
●methylated and ○unmethylated *Sma*I/*Xma*I sites CC**C**GGG

*Sma*I digestion of **unmethylated**
DNA results in fragments starting with
GGG signature

*Xma*I digestion of **methylated**
DNA results in fragments
starting with **CCGGG signature**

3’ recesses filled in

Sequencing of multiple digital signatures for each *Sma*I/*Xma*I site
Mapping to the cat genome (felCat9)

DNA methylation level for each *Sma*I/*Xma*I site
Correction by artificial methylation standards

Fig.2

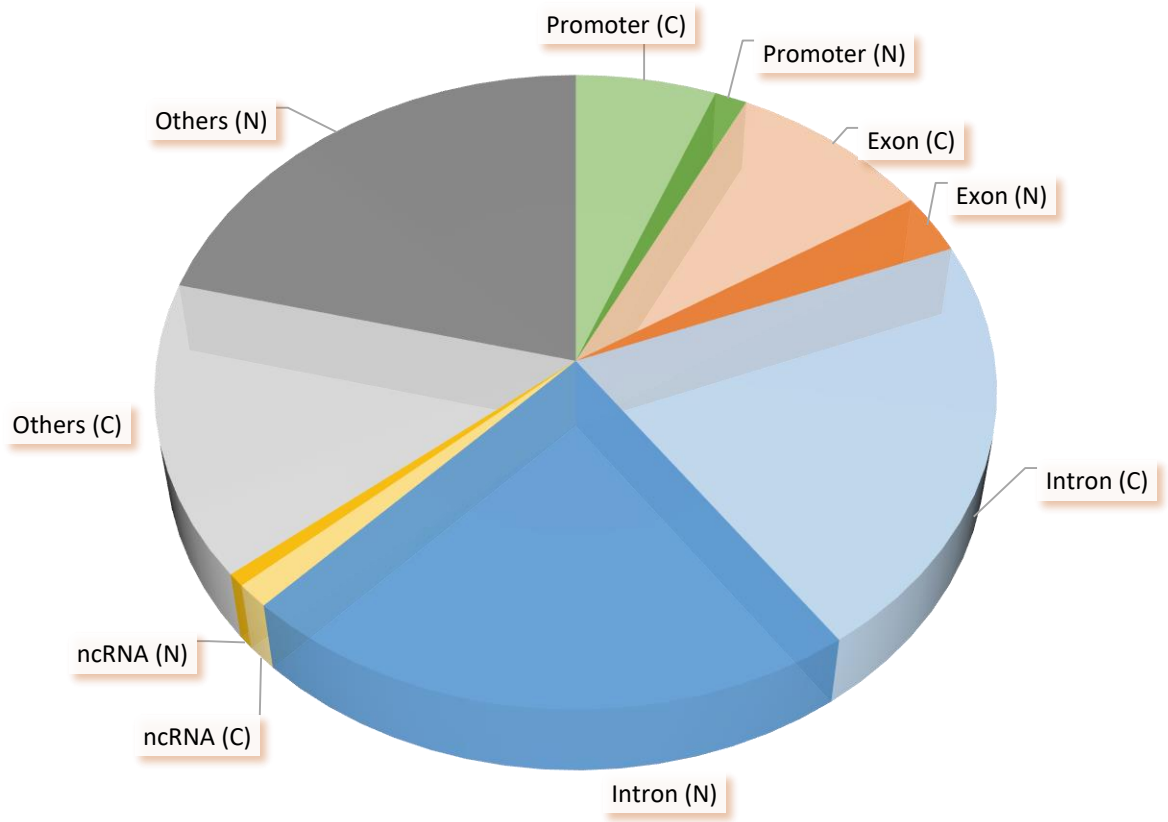

	CGI (C)	NCGI (N)	Total
Promoter	2310	533	2843
Exon	3362	1175	4537
Intron	8271	8540	16811
ncRNA	476	254	730
Others	5823	8186	14009
Total	20242	18688	38930

Fig.3

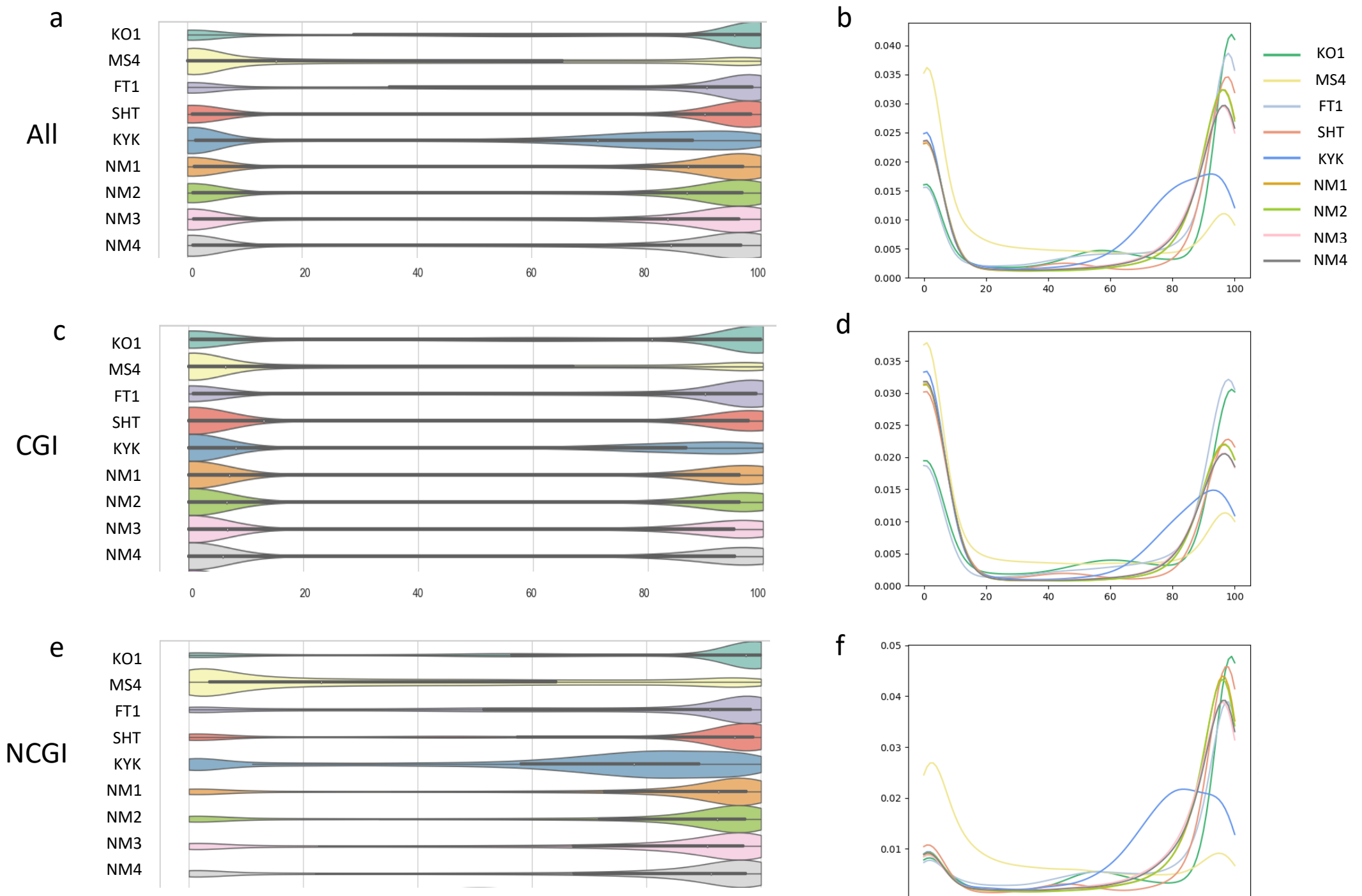
a
All
KO1
MS4
FT1
SHT
KYK
NM1
NM2
NM3
NM4
0
20
40
60
80
100
b
0.040
0.035
0.030
0.025
0.020
0.015
0.010
0.005
0.000
c
CGI
d
e
NCGI
f
0.05
0.04
0.03
0.02
0.01

Fig.4

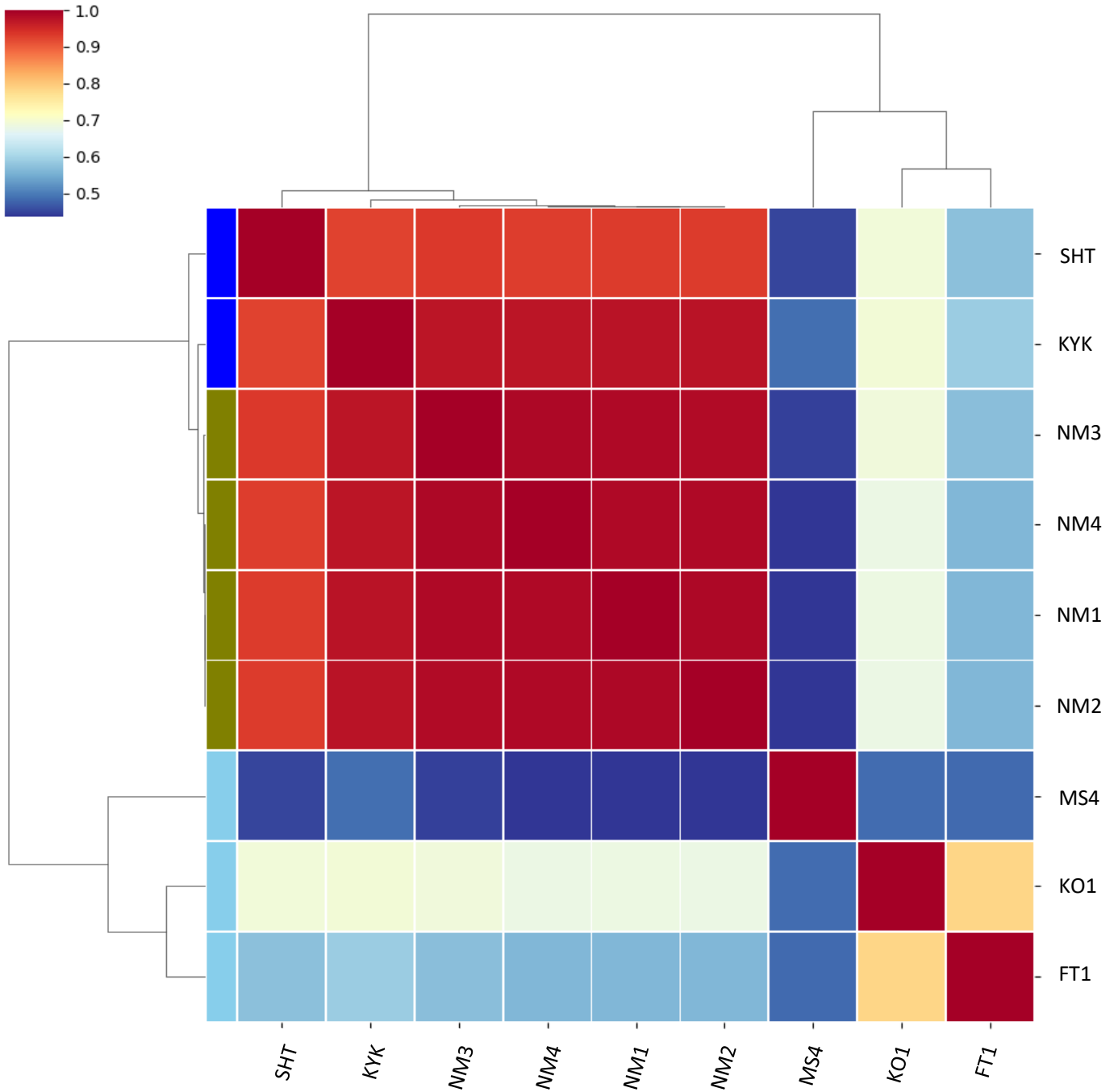
1.0
0.9
0.8
0.7
0.6
0.5
SHT
KYK
NM3
NM4
NM1
NM2
MS4
KO1
FT1
SHT
KYK
NM3
NM4
NM1
NM2
MS4
KO1
FT1

Fig.5

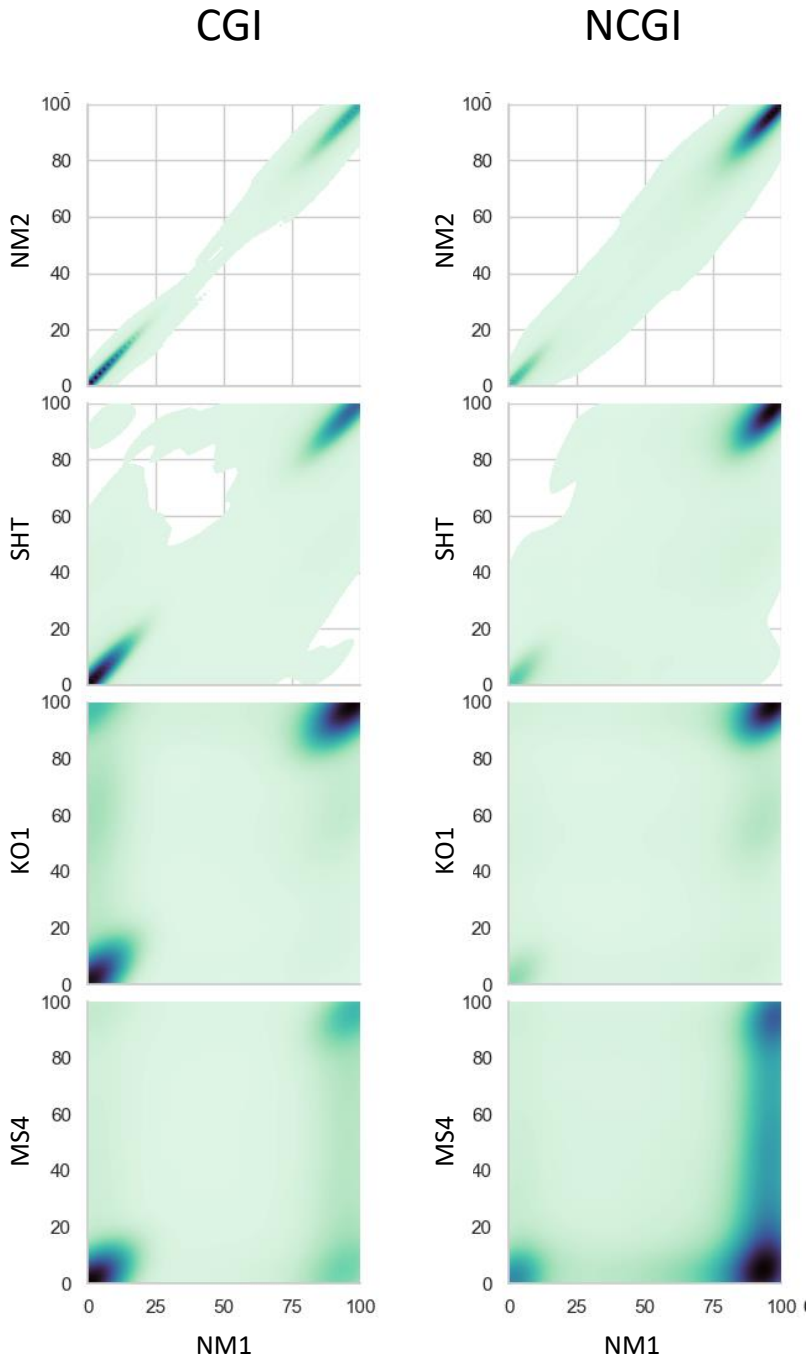

Fig.6

A

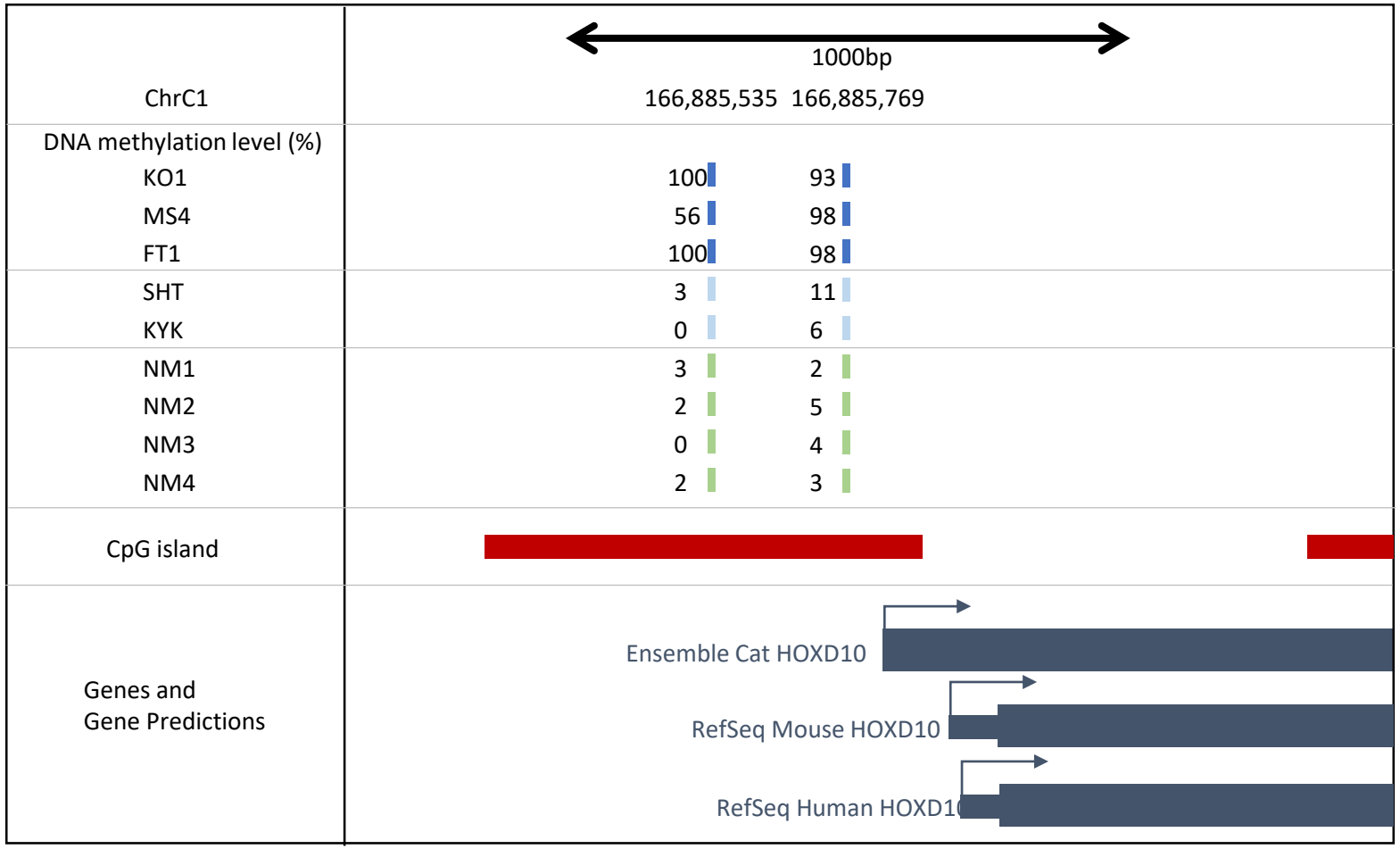
1000bp
ChrC1
166,885,535 166,885,769
DNA methylation level (%)
KO1 100 93
MS4 56 98
FT1 100 98
SHT 3 11
KYK 0 6
NM1 3 2
NM2 2 5
NM3 0 4
NM4 2 3
CpG island
Genes and
Gene Predictions
Ensemble Cat HOXD10
RefSeq Mouse HOXD10
RefSeq Human HOXD1

B

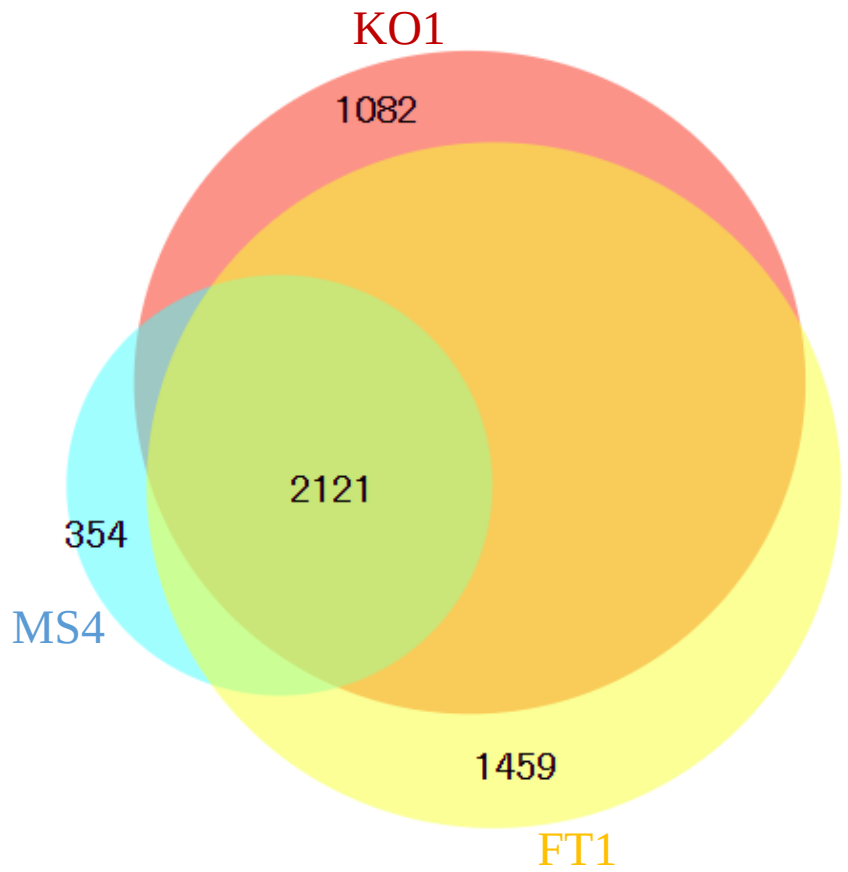
KO1
1082
2121
354
MS4
1459
FT1